Talanta 215 (2020) 120791

Contents lists available at ScienceDirect

Talanta

journal homepage: www.elsevier.com/locate/talanta

Electronic classification of barcoded particles for multiplexed detection using supervised machine learning analysis

Jianye Sui, Pengfei Xie, Zhongtian Lin, Mehdi Javanmard*

Department of Electrical and Computer Engineering, Rutgers University, Piscataway, NJ, 08854, USA

ARTICLE INFO

Keywords:
Electronically barcoded particles
Biosensor
Electrical impedance
Support vector machine
Biomarker

ABSTRACT

Wearable biosensors are of great interest in recent years due to their potential in health related applications. Multiplex biomarker analysis is needed in wearable devices to improve the sensitivity and reliability. Electronic barcoding of micro-particles has the possibility to enable multiplexed biomarker analysis. Compared with traditional optical and plasmonic methods for barcoding, electronically barcoded particles can be classified using ultra-compact electronic readout platforms. Nano-electronic barcoding works by depositing a thin layer of oxide on the top half of a micro-particle. The thickness and dielectric property of the oxide layer can be tuned to modulate the frequency dependent impedance signature of the particles. A one to one correspondence between a target biomarker and each barcoded particle can potentially be established using this technique. The barcoded particles could be tested with wearable devices to enable multiplex analysis for portable point-of-care diagnostics and real-time monitoring. In this work, we fabricated nine barcoded particles by forming oxide layers of different thicknesses and different dielectric materials using atomic layer deposition and assessed the ability to accurately classify particle barcodes using multi-frequency impedance cytometry in conjunction with supervised machine learning.

1. Introduction

Wearable devices can enable continuous real-time monitoring and assessment by analyzing biomarkers non-invasively [1–4]. Biomarker-based analysis has the potential to enable early disease diagnosis, prognosis, health monitoring, therapy management, and also drug toxicity [5–8]. Given the heterogeneity across the population in various disease conditions, the analysis of a multitude of biomarkers in wearable biosensor devices using multiplexing technologies is necessary for improving sensitivity and selectivity of diagnosis [9–11].

Two general modalities available for detection of biomarkers include optical and electrical detection. Optical detection technologies are typically more sensitive by nature compared to their electrical counterparts and have enabled high throughput multiplexing through use of various barcoding methods. However, the instrumentation tends to have a large footprint, thus is more suitable for benchtop applications [12–15]. Common techniques used for particle barcoding include photo-patterning [16,17], the use of fluorescent colloids [18,19], and semiconductor quantum dots [20–23]. These technologies have been demonstrated for multiplex analysis of nucleic acids [24] and proteins [25]. The Luminex platform is a commercially available benchtop instrument for high-throughput multiplexed biomarker analysis which uses two-photon excitation of fluorescent magnetic microspheres [26,27].

On the other hand, electrical impedance and electrochemical-based techniques are usually low cost, low power, lightweight, and easy to miniaturize. While various electrical technologies have been developed for highly sensitive biomarker analysis [28–30], they lagged behind their optical counterparts in terms of throughput due to the lack of suitable methods for barcoding particles. The most straight forward method for impedance based multiplex analysis would involve utilization of beads of different sizes, however variations in fabrication, along with bead aggregation would limit the ultimate throughput. Previously, we (Xie et al.) presented a new impedance based barcoding approach that works by depositing tunable nano-capacitors on the surfaces of microspheres [31]. The nano-capacitor consisted of an electron beam evaporated gold layer on the top half of the sphere, and another atomic layer deposited oxide layer on top, forming a Janus particle. These barcodes utilize a well-known, but previously unexplored phenomenon of Janus particles that the Clausius-Mossotti (CM) factor spectrum shifts depending on the dielectric half of the microsphere, and also the fact that the CM factor can be obtained directly by measuring the frequency dependent impedance for each particle.

In previous work, we have developed a key component that can be

* Corresponding author. Department of Electrical and Computer Engineering, Rutgers University, New Brunswick, 94 Brett Rd, Piscataway, NJ, 08854, USA
E-mail address: mehdi.javanmard@rutgers.edu (M. Javanmard).

https://doi.org/10.1016/j.talanta.2020.120791
Received 18 September 2019; Received in revised form 8 January 2020; Accepted 28 January 2020
Available online 28 January 2020
0039-9140/

used as a module in wearable devices for biomolecular detection [32]. In this work, we develop a new fabrication method for the barcoded particles along with novel data analytics. We fabricate nine barcoded particles using varying oxide thicknesses and dielectric properties. We also report a new finding that a single thin-film dielectric layer is sufficient for particle barcoding, eliminating the need for an intermediate gold layer, thus simplifying fabrication. We performed a basic study of the fabrication parameters involved in the barcoded particles, and assessed the classification accuracy. As our approach is based on electrical detection, it has the potential to be implemented in wearable biosensors for multiplex analysis.

Recently, much interests has been shown in utilizing machine learning techniques to enhance both sensitivity and classification of biosensors [33–35]. Without being explicitly programmed, machine-learning algorithms could help classify different biomolecules. Supervised machine learning allows for training a classifier with labeled data described by many features, whereby the classifier determines the optimal boundary for accurately classifying the data. The accuracy of the classifier is then assessed using test data with known values. The support vector machine (SVM) is a broadly used supervised machine learning algorithm technique for classification and regression analysis [36,37]. We previously demonstrated the utility of machine learning in classification of drug-sensitive cancer cells.[43] In this work, we perform measurements of barcoded particles using multi-frequency impedance cytometry and utilize the amplitude of the barcoded particles at each frequency as features for the SVM classifier to enhance our ability to accurately classify particle barcodes.

2. Methods and materials

2.1. Barcoded particle fabrication

The fabrication process of barcoded particles is showed in Fig. 1. It starts with forming a single layer of 3 μm polystyrene beads on a glass substrate by drop-coating. As the liquid evaporates, the bead gradually assembles together under inter-particle forces. After wiping off the polystyrene beads accumulated on the back side, atomic layer deposition (ALD) was performed to deposit a layer of oxide on top of polystyrene beads on the front side. To avoid melting of the polystyrene particles, the operation temperature of ALD was set to 150 °C. We simplified the fabrication method by eliminating the deposition of intermediate gold layer before coating the oxide. In this work, we deposit different oxides (alumina, hafnia and titania) of different thicknesses (10 nm, 20 nm and 30 nm) on bare polystyrene beads to form different barcoded particles. At last, barcoded particles are collected in phosphate buffered saline (PBS) with ultrasonication for agitation.

2.2. Sensor design and fabrication

The sensor is designed to measure the electrical impedance of barcoded particles at multiple frequencies. It consists of two parts, sensing electrodes and a microfluidic channel, as shown in Fig. 2A and B. Two coplanar electrodes are designed as 20 μm in width and the gap between two electrodes is 30 μm. To improve the sensitivity while minimize clogging, the microfluidic channel size is set as 15 μm in height and 30 μm in width. Sensing electrodes are fabricated through a standard photolithography process on a 3 inch glass wafer. The first step is patterning the photoresist, which includes cleaning the wafer, spin coating photo resist, pre-bake, aligning the mask and wafer, exposing UV light, development, and post-bake. Then, 5 nm chromium and 100 nm gold are deposited sequentially on the wafer using electron beam evaporation. At last, unintended metal is removed by lift off process.

The microfluidic channel is fabricated using soft lithography. The channel mold is made by patterning a layer of SU-8 on a 3-inch silicon wafer using a similar process as described above. We then transfer the channel pattern from channel molding to a polydimethylsiloxane (PDMS) slab. The process includes mixing pre-polymer and curing agent at a ratio of 10:1 sufficiently, pouring the mixture onto the channel mold, degassing for 15 min to remove bubbles and baking at 80 °C around 30 min for curing. Afterwards, a 5 mm inlet well and 1.2 mm outlet well are punched. At last, the microfluidic channel is bonded onto the electrode patterned glass wafer using oxygen plasma.

2.3. Frequency-dependent impedance modulation

By depositing oxides of different materials and thicknesses on the particles, the overall frequency-dependent impedance of the particle is tuned. Previous work [31] has shown that an insulative layer can modulate the Claussius-Mossotti (CM) factor, which describes the frequency dependence of the effective polarization, given by Eq. (1).

$$f_{CM}(\omega) = \frac{\tilde{\varepsilon}_p - \tilde{\varepsilon}_m}{\tilde{\varepsilon}_p + 2\,\tilde{\varepsilon}_m} \tag{1}$$

where

$$\tilde{\varepsilon}_m = \varepsilon_m - \sigma_m / j\omega \tag{2}$$

The CM factor is determined by the complex permittivity of the barcoded particle ($\tilde{\varepsilon}_p$) and the buffer medium ($\tilde{\varepsilon}_m$). The complex permittivity consists of both the dielectric constant (ε) and conductivity (σ). The barcoded particle is asymmetric and the CM factor can be calculated as the average of CM factors of a sphere and a layered particle [38]. The complex permittivity of a layered particle is given by the following equation [39]:

$$\tilde{\varepsilon}_{eff} = \tilde{\varepsilon}_{out} \frac{\left(\frac{R_{out}}{R_{in}}\right)^3 + 2\frac{\tilde{\varepsilon}_{in} - \tilde{\varepsilon}_{out}}{\tilde{\varepsilon}_{in} + 2\tilde{\varepsilon}_{out}}}{\left(\frac{R_{out}}{R_{in}}\right)^3 - 2\frac{\tilde{\varepsilon}_{in} - \tilde{\varepsilon}_{out}}{\tilde{\varepsilon}_{in} + 2\tilde{\varepsilon}_{out}}} \tag{3}$$

where $\tilde{\varepsilon}_{eff}$ is the effective complex permittivity of entire particle, $\tilde{\varepsilon}_{out}$, $\tilde{\varepsilon}_{in}$ are the complex permittivity of the outer layer and the inner core respectively. R_{out} is the radius of the entire particle (including the inner

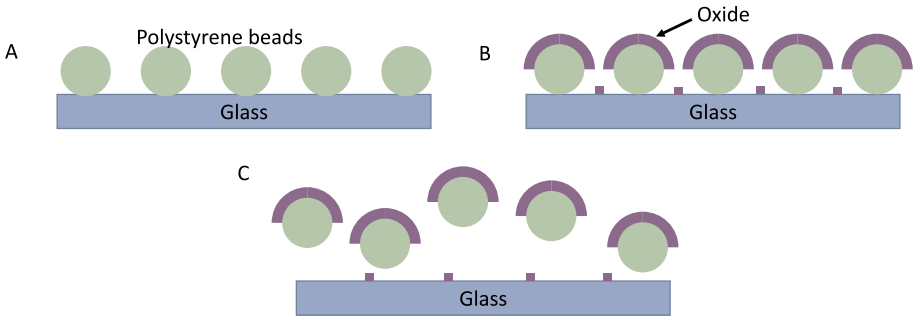

Fig. 1. Fabrication process of barcoded particles. 1) Formation of self-assembled monolayer on glass by dip-coating glass slide. 2) Deposition of oxide layer using atomic layer deposition. 3) Re-suspension of particles to solution using ultrasonication.

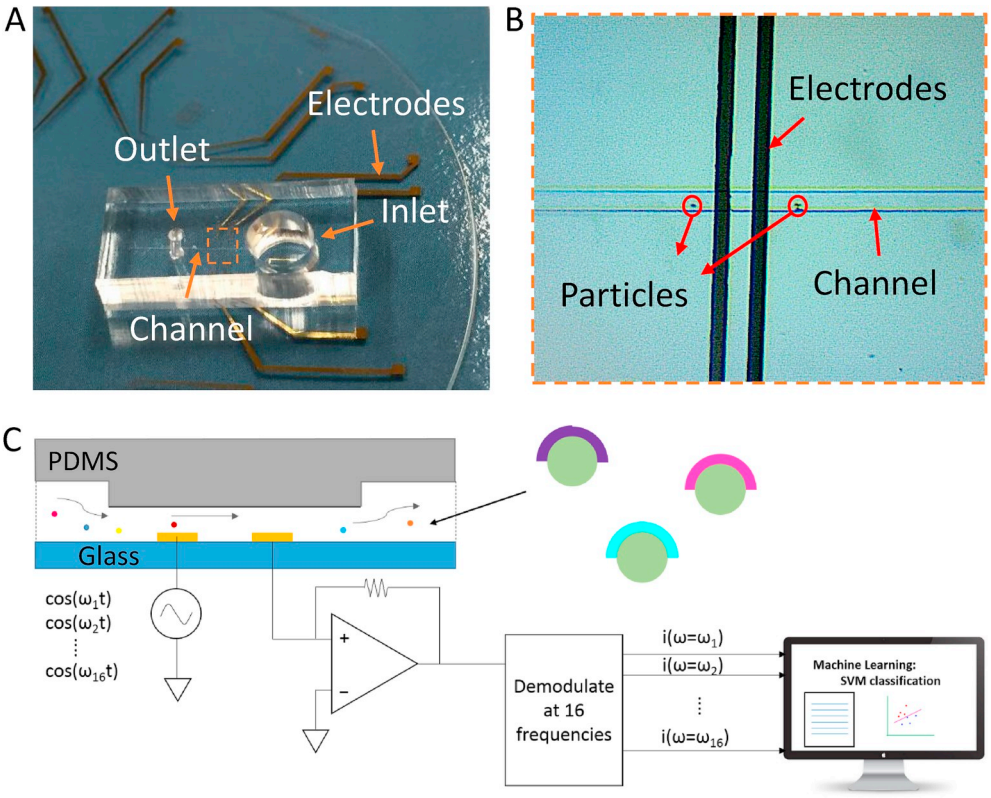

Fig. 2. Strategy overview. A) Image of the device in which a soft-lithography fabricated PDMS micro-channel is integrated with the electrode patterned on the fused silica wafer. B) Microscope image of electronic barcoded particles flowing through the sensor region. C) Schematic diagram of a multi-frequency impedance flow cytometer for classifying nanoelectronic barcoded particles. Beads are injected into the inlet well using a micro-pipette. As beads flow through the pore, the impedance change is captured by the lock-in amplifier at multiple frequencies. Data are recorded and analyzed in Matlab using a machine learning algorithm.

core) and R_{in} designates the radius of inner core. Previous studies demonstrated that the CM factor is directly related to the impedance [40]. Hence, the impedance will be affected as the CM factor is altered. This could be expressed by Eq. (4),

$$Z(\omega) = \frac{\kappa}{j\omega\tilde{\varepsilon}_m}(1 - 3\,\varphi\, f_{CM}) \tag{4}$$

where κ is a geometric constant, given by the ratio of electrode area to electrode separation and ϕ is the volume fraction occupied by the particle.

2.4. Multi-frequency impedance cytometry

Different thicknesses of the oxide layer and different oxide materials modulate the particle surface conductance, permittivity, and charging profile, thus tuning the CM factor and changing the frequency dependent impedance. Using a micro-impedance cytometer (sensor), which contains micro-electrodes integrated with a micro-channel, in conjunction with a multi-frequency lock-in amplifier (Zurich Instruments HF2A, Zurich, Switzerland), we captured the impedance responses of barcoded particles at multiple frequencies. The schematic diagram is shown in Fig. 2C. We obtain impedance data at 4 frequencies simultaneously in one measurement and implemented 4 different measurements for each type of barcoded particles (16 frequencies in total ranging from 100 kHz to 30 MHz). We limited the measurement to 4 frequencies to prevent electrodes from burning out, as more current is pumped into the electrodes per each extra frequency is added to the measurement. In each frequency measurement, 500 kHz was used as a standard frequency for control. The electrodes get stimulated by a combination of 4 different frequency AC signals generated by the lock-in amplifier.

The experiment starts by making the microfluidic channel hydrophilic using oxygen plasma. We fill the channel with PBS to preserve the hydrophilicity until the measurement begins. Particles are introduced to the channel from inlet well after removing the PBS. Under gravity and the pressure gradient in the channel, caused by the inlet and outlet fluid height difference, particles continuously flow through the channel. When the particle passes the sensing region, it partially occludes the ions conducting between electrodes and thus changes the impedance across the electrodes. This change is captured by the lock-in amplifier and the signal is demodulated at the same frequency used for stimulation. To screen the noise and interference from the environment, the device was placed in a metal box during the experiment.

2.5. Machine learning analysis

To enable better classification of different barcoded particles, we employed a standard off-the-shelf supervised machine learning classifier, the support vector machine (SVM). For each particle barcode, we performed multi-frequency impedance measurements. The peak intensity at each frequency is used as a feature. We train the SVM model with half of the data (around 200) and test with the other half data (around 200). A 5-fold cross validation is implemented to protect against overfitting. A Gaussian kernel is chosen for SVM training and testing. By comparing the predicted category and the true class, we are able to determine the accuracy of the SVM classifier, which, in turn, also depicts the impedance difference between different barcoded particles. The analysis is implemented in MATLAB (Mathworks, MA, USA) using Classification Learner toolbox.

3. Results

We fabricated different barcoded particles using atomic layer deposited oxides of varying thickness and dielectric permittivity. Nine different particles were tested, including bare polystyrene beads, polystyrene beads coated with 10 nm, 20 nm and 30 nm alumina, polystyrene beads coated with 10 nm, 20 nm and 30 nm hafnia and polystyrene beads coated with 10 nm and 20 nm titania.

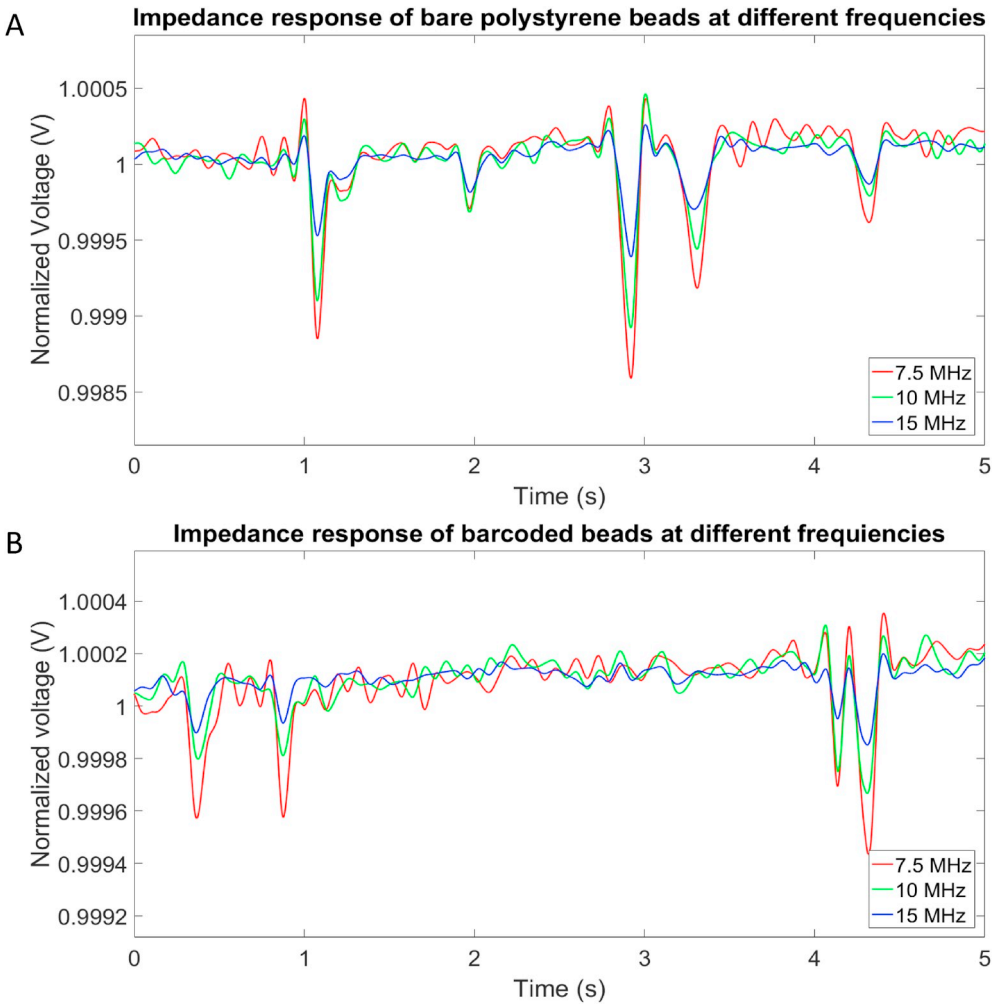

Fig. 3. Representative data of different beads passing through the sensing region measured at 7.5 MHz, 10 MHz, and 15 MHz respectively. A) Bare polystyrene beads B) Barcoded beads.

3.1. Impedance response of particles at multiple frequencies

Fig. 3 shows representative multi-frequency (7.5 MHz, 10 MHz and 15 MHz) time series data of bare polystyrene beads and polystyrene beads coated with 20 nm alumina in a time window of 5 s. The lock-in amplifier measures the current flowing out of the electrode. Then the current is converted to the voltage and the signal is demodulated at the desired frequency. Thus, the voltage is proportional to the impedance across two electrodes. The voltage is normalized to the baseline for ease of comparison. As shown in the figure, the voltage peak intensity decreases as frequency increases. This can be attributed to the surface capacitance of the beads, which gets shorted gradually as frequency increases and hence the overall impedance decreases. The barcoded particles have smaller impedance peak intensity at higher frequencies compared with bare polystyrene beads because of the larger surface capacitance [31,41]. As the data indicates, analyzing impedance at multiple frequencies can allow differentiation of barcoded particles from each other.

3.2. Effect of oxide layer thickness

We studied the effect of oxide layer thicknesses on impedance modulation. In the case of particles with a deposited alumina or hafnia layer, we studied 10 nm, 20 nm, and 30 nm. In the case of titania, we studied 10 nm and 20 nm. Fig. 4 shows the impedance responses of different materials with different thickness. The peak amplitude refers to the intensity of impedance change resulting from a particle passing through the sensing region in the channel. Different frequencies were chosen to show the best separation of different barcoded particles. Fig. 4A shows the scatter plot of peak intensities of alumina barcoded particles of 3 different thicknesses at two different frequencies (f = 500 kHz and f = 15 MHz). 20 nm alumina barcoded particles exhibit the largest voltage peak on average at 500 kHz, while 10 nm alumina barcoded particles demonstrate the largest voltage peak on average at 15 MHz. In Fig. 4B, the impedance responses of different thicknesses of hafnia at f = 500 kHz and f = 5 MHz are depicted. The impedance responses of 20 nm and 30 nm hafnia barcoded particles overlap with each other, yet they are both distinguishable from the impedance of 10 nm hafnia barcoded particles. The thickness of titania has a larger effect on impedance response, as shown in Fig. 4C. The peak amplitude of particles coated with 20 nm titania is on average larger than that of particles coated with 10 nm titania at both f = 500 kHz and f = 2 MHz. This is because the dielectric constant of titania is much larger than the other oxides, and thus result in larger impedance change for the same increase in oxide thickness compared with hafnia or alumina.

Machine learning analysis is implemented to enhance the classification ability. The bar graphs in Fig. 4D and E demonstrate the accuracy of the SVM model in differentiating between barcoded particles with the same dielectric, yet different oxide thicknesses. The accuracy in discriminating between particles coated with 10 nm titania from 20 nm titania is 96%. Overall, the SVM classifier could distinguish

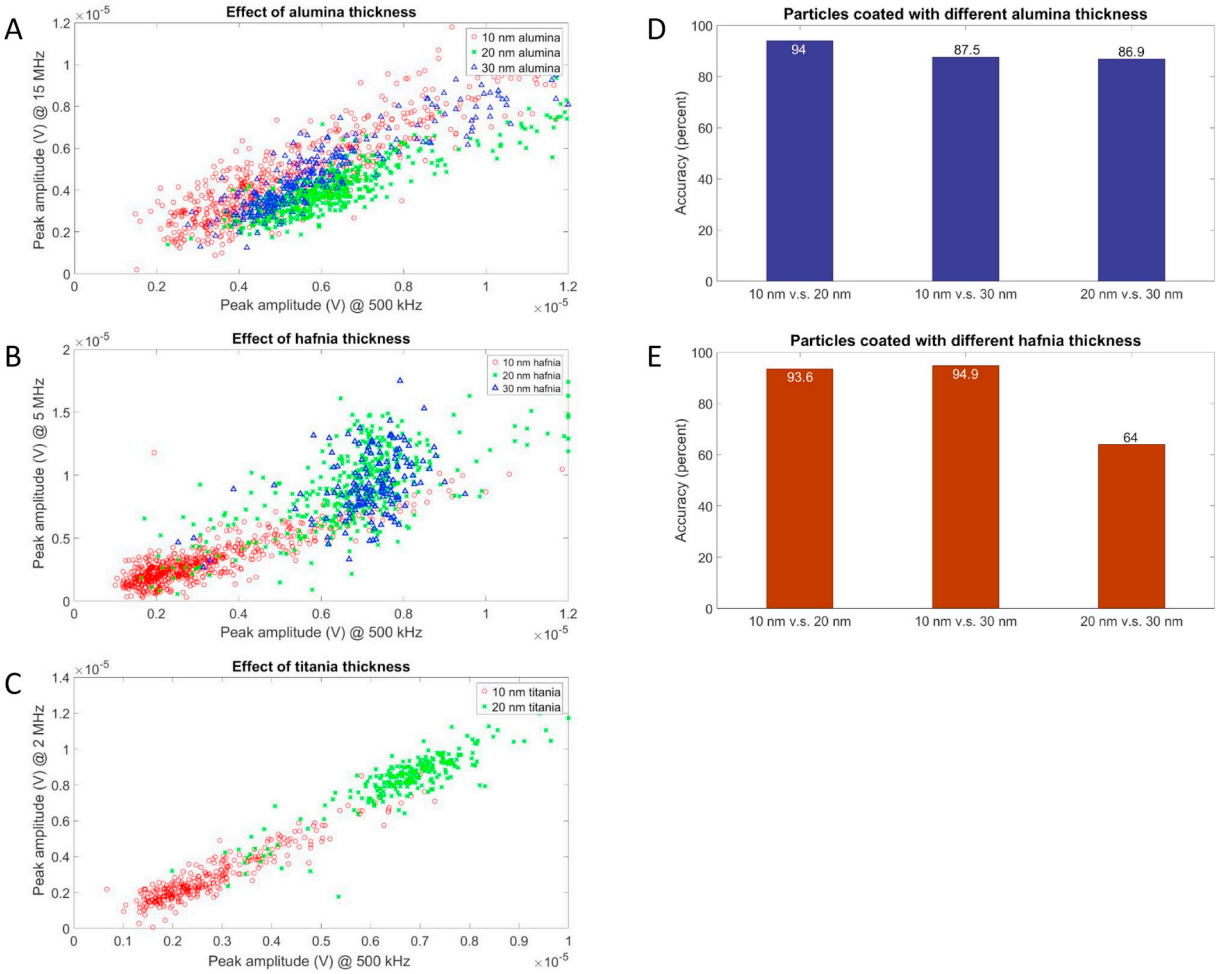

Fig. 4. The impedance responses of barcoded particles with different thickness oxides. A) Scatter plot of peak amplitude @ 500 kHz vs. peak amplitude @ 15 MHz of particles with different aluminia thickness. B) Scatter plot of peak amplitude @ 500 kHz vs. peak amplitude @ 5 MHz of particles with different hafnia thickness. C) Scatter plot of peak amplitude @ 500 kHz vs. peak amplitude @ 2 MHz of particles with different titania thickness. D) The accuracy of SVM model differentiating particles with different thickness of alumina. E) The accuracy of the SVM model differentiating particles with different thickness of hafnia.

alumina and hafnia barcoded particles from each other with high accuracy, with the exception of particles deposited with 20 nm and 30 nm hafnia, whose impedance responses also significantly overlap with each other in the scatter plot. Based on this information, it implies that when developing a multiplexed assay, it is important to properly select only the barcodes that can be classified with high levels of accuracy.

3.3. Distinction between particles coated with different dielectric layers

Besides oxide layer thickness, we also studied the effect of oxide permittivity on impedance modulation. We compared the impedance responses of particles coated with oxide layers of the same thickness but different dielectric materials. The scatter plot of peak intensity at two different frequencies is shown in Fig. 5. Different frequencies were chosen to show the best separation of different barcoded particles. In Fig. 5A, the responses of particles deposited with 10 nm of different oxides are depicted. The particles coated with alumina has the largest voltage peak amplitude on average at both 500 kHz and 20 MHz, while particles coated with hafnia or titania experience smaller current drop when spassing through the sensing region. In Fig. 5B, particles coated with 20 nm hafnia or titania show a response similar to the 10 nm situation. However, the peak intensity of particles coated with alumina is smaller than hafnia and titania at both 500 kHz and 5 MHz. In Fig. 5C, the particles coated with the 30 nm oxide layer can be easily distinguished from each other at both 500 kHz and 15 MHz.

We performed SVM analysis to quantify the ability to discriminate between barcoded particles with different dielectric layers. The accuracy in discriminating between particles coated with 30 nm alumina from 30 nm hafnia is 91%. As shown in Fig. 5D and E, the SVM result also indicates that the difference between hafnia and titania is smaller than others, which is consistent with the response seen in the scatter plots. From the results, barcoded particles with a 20 nm oxide layer can be more easily distinguished from that of a 10 nm oxide layer, which suggests we should use particles with thicker oxide layers in multiplexed analysis for better discrimination.

4. Discussion

The results presented in this paper demonstrate the ability to tune the impedance spectrum of particles by depositing insulation layers of varying thickness and dielectric materials. Supervised machine learning in conjunction with multi-frequency impedance cytometry can be used for readout and classification of the particles. The additional novelty of this work is that we demonstrated that a single thin-film dielectric layer is sufficient for particle barcoding, and one can omit the use of an intermediate gold layer, thus simplifying the fabrication process. We fabricated 9 single dielectric layer barcoded particles using this simplified process. By utilizing supervised machine learning , we enhanced the classification ability to distinguish barcoded particles. As a result, these particles can be selected and utilized as barcodes in a functional

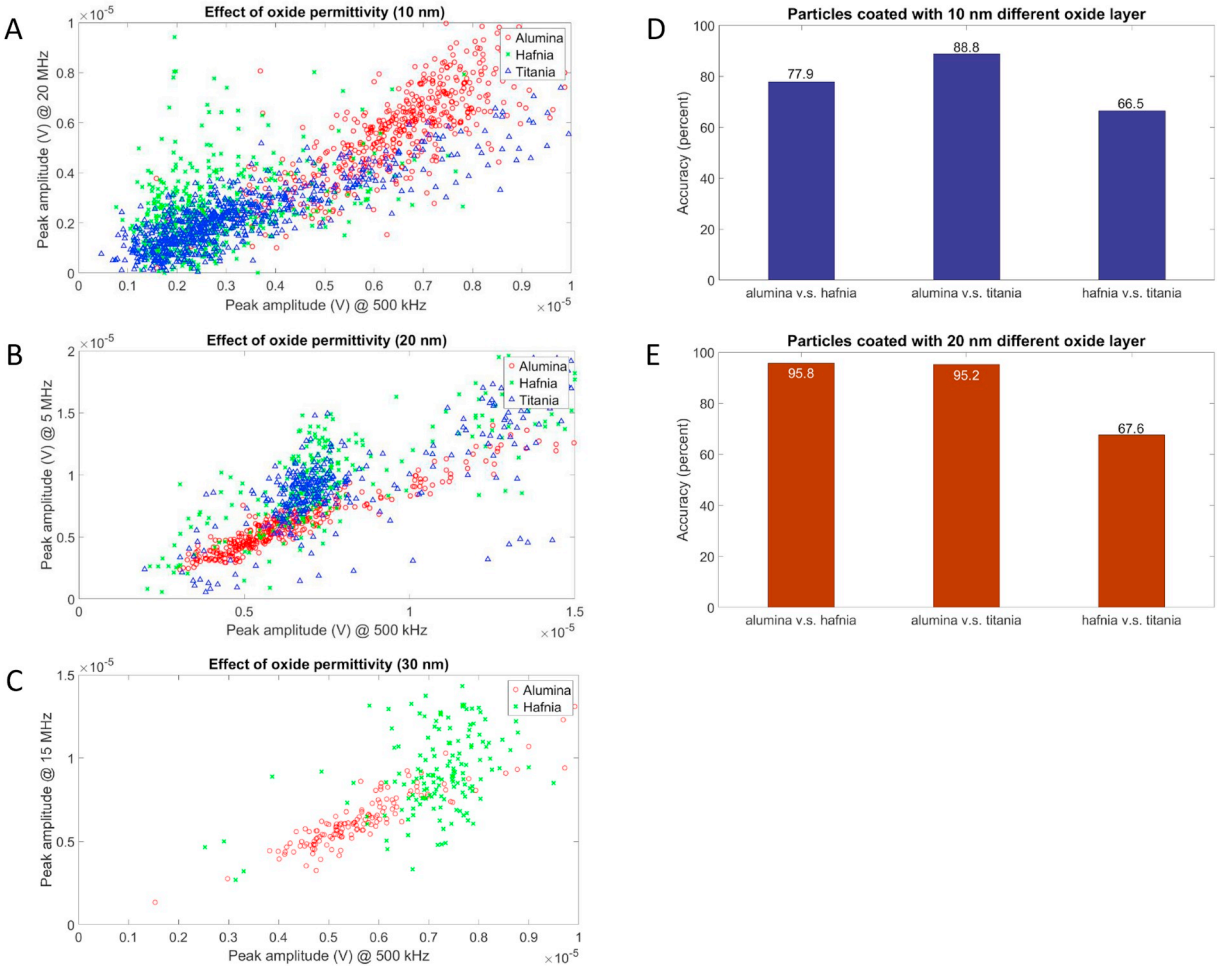

Fig. 5. The impedance responses of barcoded particles with different dielectric oxides. A) Scatter plot of peak amplitude @ 500 kHz vs. peak amplitude @ 20 MHz of particles with 10 nm different oxides. B) Scatter plot of peak amplitude @ 500 kHz vs. peak amplitude @ 5 MHz of particles with 20 nm different oxides. C) Scatter plot of peak amplitude @ 500 kHz vs. peak amplitude @ 15 MHz of particles with 30 nm different oxides. D) The accuracy of SVM model differentiating particles with 10 nm different oxides. E) The accuracy of SVM model differentiating particles with 20 nm different oxides.

biomarker assay to improve the throughput in the future.

For future work involving a multiplexed assay, our results provide guidance for selection of particles: 1) 20 nm hafnia and 30 nm hafnia particles should not be used together in the same assay. 2) Similar thickness of hafnia and titania particles should be avoided in the same assay mixture. 3) When using insulators of the same thickness but different permittivity in a single assay, 20 nm particles can provide better discrimination compared with 10 nm.

Another notable result is that the change in impedance does not necessarily change linearly with oxide thickness change. The underlying reason behind this requires further study. For particles coated with 20 nm hafnia and 30 nm hafnia, the impedance responses are similar. One possibility is that there is a threshold thickness for each dielectric, beyond which the impedance will not further change. Future efforts will be dedicated to gaining a more clear understanding of these questions and applying the particles to performing multiplex protein biomarker assays. This manuscript is focused on electronically discriminating between the different barcodes. Potential methods for quantification of the biomarkers using these barcodes has previously been discussed elsewhere [29,31,42]. The wearable platform for detection is reported in another paper [32].

5. Conclusion

In this paper, we fabricate nine barcoded particles by depositing different thicknesses and types of oxide layers on top of bare polystyrene beads. We demonstrated that a single oxide layer can sufficiently modulate the frequency dependent impedance and thus eliminate the need for the intermediate gold layer and simplify particle fabrication. A micro-impedance cytometer (sensor) was designed and fabricated to perform multi-frequency impedance cytometry, where the PDMS-based microfluidic channel was covalently bonded onto the surface of electrode glass chip. By implementing impedance measurements at multiple frequencies in conjunction with machine learning analysis, we demonstrate the capability of our sensor to detect different particle barcodes. Finally, we provide systematic guidelines for selection of particle barcodes to be used in a multiplexed biomarker assay in the future.

Declaration of competing interest

The authors declare that they have no conflict of interest.

Acknowledgements

This work was supported by National Science Foundation Award No. IDBR 1556253 and start-up funds provided to M. J. by the School of Engineering and the Department of Electrical Engineering at Rutgers, The State University of New Jersey. The devices were fabricated in the Microelectronics Research Laboratory (MERL) of Rutgers University.

References

[1] W. Gao, S. Emaminejad, H.Y.Y. Nyein, S. Challa, K. Chen, A. Peck, H.M. Fahad, H. Ota, H. Shiraki, D. Kiriya, Fully integrated wearable sensor arrays for multiplexed in situ perspiration analysis, Nature 529 (7587) (2016) 509.

[2] J. Kim, A.S. Campbell, B.E.-F. de Ávila, J. Wang, Wearable biosensors for healthcare monitoring, Nat. Biotechnol. (2019) 1.

[3] W. Gao, H.Y. Nyein, Z. Shahpar, H.M. Fahad, K. Chen, S. Emaminejad, Y. Gao, L.-C. Tai, H. Ota, E. Wu, Wearable microsensor array for multiplexed heavy metal monitoring of body fluids, ACS Sens. 1 (7) (2016) 866–874.

[4] A. Romeo, T. Leung, S. Sanchez, Smart biosensors for multiplexed and fully integrated point-of-care diagnostics, Lab Chip 16 (11) (2016) 1957–1961.

[5] B. Laxman, D.S. Morris, J. Yu, J. Siddiqui, J. Cao, R. Mehra, R.J. Lonigro, A. Tsodikov, J.T. Wei, S.A. Tomlins, A first-generation multiplex biomarker analysis of urine for the early detection of prostate cancer, Canc. Res. 68 (3) (2008) 645–649.

[6] N.R. Kitteringham, R.E. Jenkins, C.S. Lane, V.L. Elliott, B.K. Park, Multiple reaction monitoring for quantitative biomarker analysis in proteomics and metabolomics, J. Chromatogr. B 877 (13) (2009) 1229–1239.

[7] Y. Li, Q. Zheng, C. Bao, S. Li, W. Guo, J. Zhao, D. Chen, J. Gu, X. He, S. Huang, Circular RNA is enriched and stable in exosomes: a promising biomarker for cancer diagnosis, Cell Res. 25 (8) (2015) 981.

[8] H. Gao, J.M. Korn, S. Ferretti, J.E. Monahan, Y. Wang, M. Singh, C. Zhang, C. Schnell, G. Yang, Y. Zhang, High-throughput screening using patient-derived tumor xenografts to predict clinical trial drug response, Nat. Med. 21 (11) (2015) 1318.

[9] D.R. Rhodes, M.G. Sanda, A.P. Otte, A.M. Chinnaiyan, M.A. Rubin, Multiplex biomarker approach for determining risk of prostate-specific antigen-defined recurrence of prostate cancer, J. Natl. Cancer Inst. 95 (9) (2003) 661–668.

[10] J.-H. Kang, H. Vanderstichele, J.Q. Trojanowski, L.M. Shaw, Simultaneous analysis of cerebrospinal fluid biomarkers using microsphere-based xMAP multiplex technology for early detection of Alzheimer's disease, Methods 56 (4) (2012) 484–493.

[11] S. Chutipongtanate, K.D. Greis, Multiplex biomarker screening assay for urinary extracellular vesicles study: a targeted label-free proteomic approach, Sci. Rep. 8 (1) (2018) 15039.

[12] Y. Leng, K. Sun, X. Chen, W. Li, Suspension arrays based on nanoparticle-encoded microspheres for high-throughput multiplexed detection, Chem. Soc. Rev. 44 (15) (2015) 5552–5595.

[13] M. Seydack, Nanoparticle labels in immunosensing using optical detection methods, Biosens. Bioelectron. 20 (12) (2005) 2454–2469.

[14] B.J. Battersby, G.A. Lawrie, A.P. Johnston, M. Trau, Optical barcoding of colloidal suspensions: applications in genomics, proteomics and drug discovery, Chem. Commun. (14) (2002) 1435–1441.

[15] Y. Zhao, H.C. Shum, H. Chen, L.L. Adams, Z. Gu, D.A. Weitz, Microfluidic generation of multifunctional quantum dot barcode particles, J. Am. Chem. Soc. 133 (23) (2011) 8790–8793.

[16] K. Braeckmans, S.C. De Smedt, C. Roelant, M. Leblans, R. Pauwels, J. Demeester, Encoding microcarriers by spatial selective photobleaching, Nat. Mater. 2 (3) (2003) 169.

[17] H. Lee, J. Kim, H. Kim, J. Kim, S. Kwon, Colour-barcoded magnetic microparticles for multiplexed bioassays, Nat. Mater. 9 (9) (2010) 745.

[18] H. Li, X. Sun, Fluorescence-enhanced nucleic acid detection: using coordination polymer colloids as a sensing platform, Chem. Commun. 47 (9) (2011) 2625–2627.

[19] B.J. Battersby, D. Bryant, W. Meutermans, D. Matthews, M.L. Smythe, M. Trau, Toward larger chemical libraries: encoding with fluorescent colloids in combinatorial chemistry, J. Am. Chem. Soc. 122 (9) (2000) 2138–2139.

[20] J.M. Klostranec, Q. Xiang, G.A. Farcas, J.A. Lee, A. Rhee, E.I. Lafferty, S.D. Perrault, K.C. Kain, W.C. Chan, Convergence of quantum dot barcodes with microfluidics and signal processing for multiplexed high-throughput infectious disease diagnostics, Nano Lett. 7 (9) (2007) 2812–2818.

[21] M.A. Walling, J.A. Novak, J.R. Shepard, Quantum dots for live cell and in vivo imaging, Int. J. Mol. Sci. 10 (2) (2009) 441–491.

[22] Y. Zhao, X. Zhao, B. Tang, W. Xu, J. Li, J. Hu, Z. Gu, Quantum-dot-tagged bioresponsive hydrogel suspension array for multiplex label-free DNA detection, Adv. Funct. Mater. 20 (6) (2010) 976–982.

[23] N. Hildebrandt, Biofunctional quantum dots: controlled conjugation for multiplexed biosensors, ACS Nano 5 (7) (2011) 5286–5290.

[24] S.C. Chapin, P.S. Doyle, Ultrasensitive multiplexed microRNA quantification on encoded gel microparticles using rolling circle amplification, Anal. Chem. 83 (18) (2011) 7179–7185.

[25] D.C. Appleyard, S.C. Chapin, R.L. Srinivas, P.S. Doyle, Bar-coded hydrogel microparticles for protein detection: synthesis, assay and scanning, Nat. Protoc. 6 (11) (2011) 1761.

[26] M.Y. Liu, A.M. Xydakis, R.C. Hoogeveen, P.H. Jones, E.B. Smith, K.W. Nelson, C.M. Ballantyne, Multiplexed analysis of biomarkers related to obesity and the metabolic syndrome in human plasma, using the Luminex-100 system, Clin. Chem. 51 (7) (2005) 1102–1109.

[27] A. Bhimji, L. Singer, D. Kumar, A. Humar, R. Pavan, H. Zhang, C. Rotstein, S. Keshavjee, T. Mazzulli, S. Husain, Feasibility of detecting fungal DNA in exhaled breath condensate by the Luminex Multiplex xTAG fungal PCR assay in lung transplant recipients: a pilot study, J. Heart Lung Transplant. 35 (4) (2016) S37.

[28] H. Cai, T.M.-H. Lee, I.-M. Hsing, Label-free protein recognition using an aptamer-based impedance measurement assay, Sensor. Actuator. B Chem. 114 (1) (2006) 433–437.

[29] Z. Lin, X. Cao, P. Xie, M. Liu, M. Javanmard, PicoMolar level detection of protein biomarkers based on electronic sizing of bead aggregates: theoretical and experimental considerations, Biomed. Microdevices 17 (6) (2015) 119.

[30] B. Kavosi, A. Salimi, R. Hallaj, F. Moradi, Ultrasensitive electrochemical immunosensor for PSA biomarker detection in prostate cancer cells using gold nanoparticles/PAMAM dendrimer loaded with enzyme linked aptamer as integrated triple signal amplification strategy, Biosens. Bioelectron. 74 (2015) 915–923.

[31] P. Xie, X. Cao, Z. Lin, M. Javanmard, Top-down fabrication meets bottom-up synthesis for nanoelectronic barcoding of microparticles, Lab Chip 17 (11) (2017) 1939–1947.

[32] A. Furniturewalla, M. Chan, J. Sui, K. Ahuja, M. Javanmard, Fully integrated wearable impedance cytometry platform on flexible circuit board with online smartphone readout, Microsystems & Nanoengineering 4 (1) (2018) 20.

[33] H. Song, Y. Wang, J.M. Rosano, B. Prabhakarpandian, C. Garson, K. Pant, E. Lai, A microfluidic impedance flow cytometer for identification of differentiation state of stem cells, Lab Chip 13 (12) (2013) 2300–2310.

[34] H.C. Koydemir, S. Feng, K. Liang, R. Nadkarni, D. Tseng, P. Benien, A. Ozcan, A Survey of Supervised Machine Learning Models for Mobile-Phone Based Pathogen Identification and Classification, Optics and Biophotonics in Low-Resource Settings III, International Society for Optics and Photonics, 2017, p. 100550A.

[35] H.C. Koydemir, Z. Gorocs, D. Tseng, B. Cortazar, S. Feng, R.Y.L. Chan, J. Burbano, E. McLeod, A. Ozcan, Rapid imaging, detection and quantification of Giardia lamblia cysts using mobile-phone based fluorescent microscopy and machine learning, Lab Chip 15 (5) (2015) 1284–1293.

[36] Y. Zuo, S. Chakrabartty, Z. Muhammad-Tahir, S. Pal, E.C. Alocilja, Spatio-temporal processing for multichannel biosensors using support vector machines, IEEE Sensor. J. 6 (6) (2006) 1644–1651.

[37] J. Guo, Z. Chen, Y.-L. Ban, Y. Kang, Precise enumeration of circulating tumor cells using support vector machine algorithm on a microfluidic sensor, IEEE Transactions on Emerging Topics in Computing 5 (4) (2017) 518–525.

[38] L. Zhang, Y. Zhu, Dielectrophoresis of Janus particles under high frequency ac-electric fields, Appl. Phys. Lett. 96 (14) (2010) 141902.

[39] A. Irimajiri, T. Hanai, A. Inouye, A dielectric theory of "multi-stratified shell" model with its application to a lymphoma cell, J. Theor. Biol. 78 (2) (1979) 251–269.

[40] A. Valero, T. Braschler, P. Renaud, A unified approach to dielectric single cell analysis: impedance and dielectrophoretic force spectroscopy, Lab Chip 10 (17) (2010) 2216–2225.

[41] J. Sui, P. Xie, Z. Lin, M. Javanmard, Multiplexed Molecular Biomarker Analysis Using an Expanded Library of Nanoelectronically Barcoded Particles Enabled through Machine Learning Analysis, IEEE Micro Electro Mechanical Systems (MEMS), 2018, pp. 444–447 IEEE, 2018.

[42] J. Mok, M.N. Mindrinos, R.W. Davis, M. Javanmard, Digital microfluidic assay for protein detection, Proc. Natl. Acad. Sci. Unit. States Am. 111 (6) (2014) 2110–2115.

[43] K. Ahuja, G.M. Rather, Z. Lin, J. Sui, P. Xie, T. Le, J.R. Bertino, M. Javanmard, Toward point-of-care assessment of patient response: a portable tool for rapidly assessing cancer drug efficacy using multifrequency impedance cytometry and supervised machine learning, Microsyst. Nanoeng. 5 (34) (2019), https://doi.org/10.1038/s41378-019-0073-2.